Metal–Organic Frameworks

DOI: 10.1002/ange.201003377

Single-Crystal to Single-Crystal Cross-Linking of an Interpenetrating Chiral Metal–Organic Framework and Implications in Asymmetric Catalysis**

*Liqing Ma, Chuan-De Wu, Marcela M. Wanderley, and Wenbin Lin**

Metal–organic frameworks (MOFs) have received extensive interest in the past decade because of their interesting properties.[1] MOFs exhibit exceptional gas-uptake capacity owing to their extreme porosity.[2] The ability to incorporate desired functional groups allows MOFs to perform in a variety of applications, such as catalysis,[3] chemical sensing,[4] and drug delivery.[5] In particular, MOFs represent ideal candidates as heterogeneous catalysts by simultaneously imparting porosity and introducing catalytic sites into MOFs. Unlike other catalyst heterogenization strategies, the MOF-derived heterogeneous catalysts can remain single-crystalline, thus providing a unique opportunity for detailed structural interrogation and therefore delineating the relationships between the MOF structures and their catalytic activities and selectivities.

Moderate hydrolytic and thermal stabilities of most MOFs limit the scope of reactions that can be heterogeneously catalyzed by MOFs. We have recently focused our efforts on the design of chiral porous MOFs for heterogeneous asymmetric catalysis as most asymmetric catalytic reactions are carried out under mild conditions in aprotic solvents.[6] In order for chiral MOFs to be useful asymmetric catalysts, they must possess large nanometer-scale open channels for the facile transport of sterically demanding substrates and products. We have recently synthesized isoreticular chiral MOFs based on tetracarboxylate bridging ligands derived from 1,1′-bi-2-naphthol (BINOL) and copper paddle-wheel secondary building units (SBUs), and observed the remarkable dependence of the enantioselectivities of the addition of Et_2Zn to aromatic aldehydes on the MOF open-channel sizes.[7] In order to expand the scope of applications of such chiral tetracarboxylate ligands, and to further understand the relationships between framework structures and catalytic activities, we have used these ligands in combination with other metal-connecting points or metal-cluster SBUs. Herein we report the synthesis and characterization of two interpenetrating chiral MOFs $[Zn_2(L)(dmf)(H_2O)]\cdot 2\,EtOH\cdot 4.3\,DMF\cdot H_2O$ (**1**, where L is (*R*)-2,2′-diethoxy-1,1′-binaphthyl-4,4′,6,6′-tetrabenzoate) and $[Zn_2(L')(dmf)(H_2O)]\cdot 2\,EtOH\cdot 4.3\,DMF\cdot 4\,H_2O$ (**2**, L′ = (*R*)-2,2′-dihydroxy-1,1′-binaphthyl-4,4′,6,6′-tetrabenzoate), which are constructed from dizinc SBUs and chiral tetracarboxylate ligands. More importantly, we observed unprecedented single-crystal to single-crystal crosslinking of the two interpenetrating networks in **2** by $Ti(OiPr)_4$ to lead to intermolecular [Ti(BINOLate)$_2$] complexes that exhibit modest enantioselectivity in catalyzing the addition of diethylzinc to aromatic aldehydes to afford chiral secondary alcohols. This result provides unambiguous structural identification of an immobilized homogeneous catalyst and has significant implications in rational design of MOF-based heterogeneous asymmetric catalysts.

MOF **1** was synthesized by heating a mixture of ZnI_2 and (*R*)-H_4L in DMF/EtOH at 90 °C for five days, while MOF **2** was produced by heating ZnI_2 and (*R*)-H_4L′ in DMF/EtOH at 100 °C for one week (Scheme 1). The formulae of **1** and **2** were established by single-crystal X-ray diffraction studies, NMR analysis, and thermogravimetric analysis (TGA).

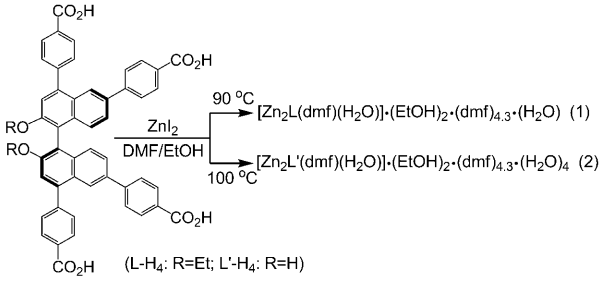

Scheme 1. Synthesis of homochiral MOFs **1** and **2**.

Crystals of **1** and **2** are isostructural and crystallize in the orthorhombic $I2_12_12_1$ space group.[8] Here we only discuss structure **2**, which contains two Zn atoms, one L′ ligand, one water molecule, and one DMF molecule in the framework in each asymmetric unit. The two Zn atoms have distinct coordination environments: one atom coordinates to four carboxyl oxygen atoms of four different L′ ligands and one water molecule in square-pyramidal geometry, and the other atom coordinates to three carboxyl oxygen atoms and one DMF molecule in a distorted tetrahedral geometry. The two distinct Zn atoms are triply bridged by carboxylate groups to

[*] Dr. L. Ma,[+] Dr. C.-D. Wu,[+] M. M. Wanderley, Prof. W. Lin
Department of Chemistry, CB#3290
University of North Carolina
Chapel Hill, NC 27599 (USA)
Fax: (+1) 919-962-2388
E-mail: wlin@unc.edu
Homepage:
http://www.chem.unc.edu/people/faculty/linw/wlindex.html

[+] These authors contributed equally to this work.

[**] We thank NSF (CHE-0809776) for financial support and Kathryn deKrafft and Dr. Banu Kesanli for experimental help.

Supporting information for this article is available on the WWW under http://dx.doi.org/10.1002/anie.201003377.

form $\{Zn_2(\mu_2\text{-}CO_2)_3(\mu_1\text{-}CO_2)\}$ SBUs. The fourth carboxylate group of L′ coordinates to the square-pyramidal Zn atom in a monodentate fashion. Consequently, each L′ ligand, as well as each Zn_2 unit, acts as a four-connecting linker that leads to a 3D network (Figure 1). Topological analysis of **2** reveals a four-connected uninodal net with a Schläfli symbol of $\{6^6\}$, which is a known topological type of *unc* (one of the uninodal 4-connected 3D nets).[9]

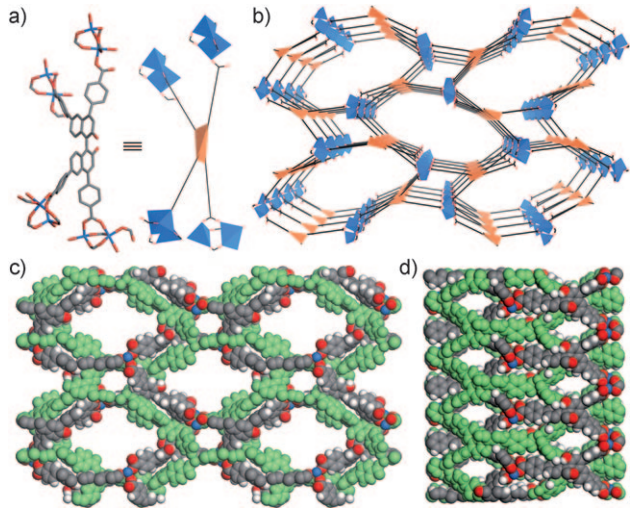

Figure 1. a) Representation of coordination modes of ligand L′ (simplified as a distorted orange tetrahedron) with zinc atoms (blue polyhedron); b) schematic representation of the network connectivity of **2** as viewed down the *a* axis; c, d) space-filling model of **2** as viewed down the *a* and *b* axis, respectively. Zn blue, O red, C gray, H white; all atoms of the other interpenetrating network are shown in green.

The non-interpenetrating *unc* network of **2** possesses an extremely large void space with the largest channel dimensions of approximately $1.5 \times 3.0\ nm^2$ along the *a* axis. To avoid the formation of such an open structure, **2** forms a twofold interpenetrated network (Figure 1c). The shortest distance between the naphthyl rings of the two interpenetrating networks is 4.05(2) Å. Even after twofold interpenetration, **2** still possesses large channels (ca. $1.5 \times 2.0\ nm^2$) along the *a* axis. PLATON calculations indicate that the effective volume for solvent molecules in framework **1** is 7932.7 $Å^3$ per unit cell, which is 49.2% of the crystal volume. Compound **2** has a void space of 7825.5 $Å^3$ per unit cell, which is 51.6% of the unit-cell volume. TGA analyses indicated solvent weight losses of 34.9% and 38.8% for **1** and **2**, respectively.

The phase purity of **1** and **2** is supported by a good match between powder X-ray diffraction (PXRD) patterns of bulk samples of **1** and **2** and those simulated from their single-crystal structures. The evacuated sample of **2** shows peak broadening at 2θ values larger than 15°, thus suggesting slight framework distortion upon solvent removal; this phenomenon is not uncommon for MOFs with elongated ligands.[10] The crystallinity of **1** and **2** is recovered after soaking the desolvated samples in a DMF/EtOH (1:1 v/v) solvent mixture for 24 h at room temperature (Figure 2). In spite of framework distortion, **1** and **2** are highly porous, as shown by N_2 and H_2 adsorption experiments.

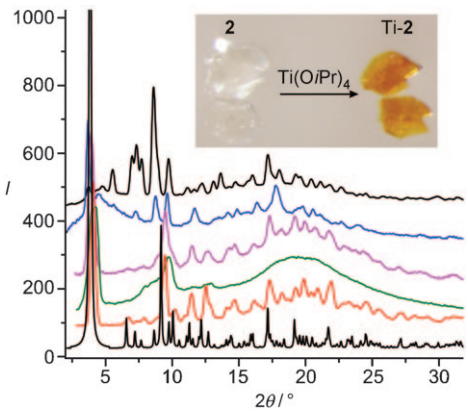

Figure 2. X-ray powder diffraction patterns for **2**. From bottom to top: simulated PXRD from the crystal structure; pristine sample; evacuated sample; evacuated sample resoaked in DMF/EtOH; sample treated with $Ti(OiPr)_4$ (denoted as Ti-loaded); and sample recovered after the catalytic Et_2Zn addition reaction. The inset shows photographs of colorless **2** and orange Ti-**2**.

The N_2 gas-sorption isotherms were measured at 77 K in order to evaluate the permanent porosity of **1** and **2**. Fresh crystals of **1** or **2** were washed with a DMF/EtOH (1:1 v/v) mixture followed by a brief wash with CH_2Cl_2. Compound **1** or **2** was then evacuated at 60 °C for 16 h under vacuum to remove the remaining solvent molecules before N_2 adsorption measurements. As shown in Figure 3, both **1** and **2** show type I

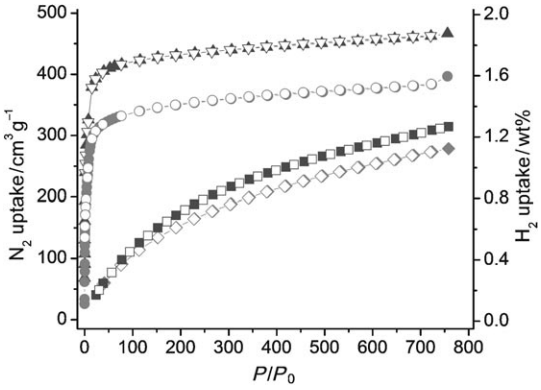

Figure 3. N_2 (●, ▲ = **2**) and H_2 (◆, ■ = **2**) adsorption (filled symbols)/desorption (open symbols) isotherms of **1** and **2** at 77 K.

adsorption isotherms, thus indicating microporous structure for these frameworks. By assuming a monolayer coverage of N_2 and applying the Langmuir model, we found that the apparent Langmuir surface areas of evacuated samples of **1** and **2** are 1481 $m^2 g^{-1}$ and 1847 $m^2 g^{-1}$, respectively (the $P/P_0 =$ 0.001 to 0.1 pressure range was selected). The BET surface area is 1335 $m^2 g^{-1}$ for **1** and 1657 $m^2 g^{-1}$ for **2**. The calculated BET surface areas based on grand canonical Monte Carlo (GCMC) simulations are 1720 $m^2 g^{-1}$ and 1877 $m^2 g^{-1}$ for **1** and **2**, respectively (Figures S5 and S7 in the Supporting Information). The structural distortion of desolvated samples

of **1** and **2** is supported by the smaller observed pore sizes, which are reduced by approximately 2 Å compared to those calculated from GCMC simulations (Figures S6 and S8 in the Supporting Information). To further characterize the gas-sorption properties of **1** and **2**, hydrogen-uptake experiments were carried out. At 1 atm and 77 K, **1** and **2** exhibit high hydrogen uptakes of 1.1 and 1.3 wt%, respectively.

We have also evaluated the accessibility of the open channels in **1** and **2** to large molecules, as this factor is important for asymmetric catalytic reactions. The uptake of Brilliant Blue R-250 dye by **1** and **2** are 8.0 and 10.6 wt%. These dye uptake amounts correspond to effective dye concentrations of 131 and 167 mM in the open channels of **1** and **2**, as compared to a dye concentration of 24 mM in the original MeOH solution. The fact that **1** and **2** can host a dye molecule with approximate dimensions of $1.8 \times 2.2\ nm^2$ suggests their ability to transport large substrate and product molecules in asymmetric catalytic reactions.

We evaluated potential applications of **2** in heterogeneous asymmetric catalysis. The dihydroxy groups in **2** can be transformed into an active Lewis acidic catalyst by post-synthesis modification with $Ti(OiPr)_4$.[6,7,11] As shown in Table 1, $Ti(OiPr)_4$-treated **2** is highly active in the addition

Table 1: Addition of diethylzinc to aromatic aldehydes catalyzed by **2**/$Ti(OiPr)_4$.[a]

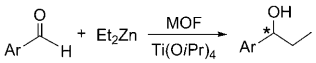

Entry	Ar	Conv. [%]	*ee* [%]
1	Ph	99	17.4
2	4-Cl-C_6H_4	99	12.1
3	4-Br-C_6H_4	99	11.1
4	1-naphthyl	98	21.8
5[b]	Ph	99	29.8
6[c]	Ph	99	< 2

[a] Reactions were carried out in toluene (1 mL), with 13 mol% of **2** with respect to the amount of BINOL. [b] With 39 mol% of **2**. [c] With 13 mol% of **1**.

of diethylzinc to aromatic aldehydes to afford secondary alcohols. However, only very modest enantioselectivity was observed in these reactions (17.4% *ee* for benzaldehyde at 13 mol% catalyst loading). This result is in stark contrast to our earlier results from MOF-catalyzed diethylzinc additions, which gave very high *ee* values (up to 93% *ee*), which rival the values obtained with corresponding homogeneous catalysts.[6,7]

Structural analysis and dye-uptake studies indicated that the channels of the doubly interpenetrating networks in **2** are accessible to aldehyde and Et_2Zn reagents. In order to understand the origin of the low enantioselectivity, single-crystal diffraction studies were carried out on $Ti(OiPr)_4$-treated **2** (denoted as Ti-**2**), which was obtained by the treating single crystals of **2** suspended in toluene with $Ti(OiPr)_4$ for three days. Compound **2** turned to from colorless to light yellow and then orange upon treatment with $Ti(OiPr)_4$ (Figure 2, inset), as a result of ligand-to-metal charge transfer excitation in Ti^{IV} naphthoxide complexes. This color change indicates the reaction of the BINOL moieties in **2** with $Ti(OiPr)_4$ to form catalytically active titanium BINOLate species. Interestingly, when the structure of Ti-**2** was resolved, the formation of intermolecular $[Ti(BINOLate)_2]$ species by single-crystal to single-crystal crosslinking of the two interpenetrating networks in **2** was revealed (Figure 4a,b). Although a number of single-crystal to single-crystal transformations of MOFs have been reported in recent years, these results represent the first example of converting a MOF to a catalytically active material in a single-crystal to single-crystal fashion.[12,13] The proximity of the two interpenetrating networks has led to short distances between OH groups from L′ ligands in different networks, thus allowing the reaction of $Ti(OiPr)_4$ with two different BINOL moieties in the two adjacent L′ ligands to form intermolecular $[(OiPr)_2Ti(BINOLate)_2]$ complexes (Figure 4b,c). The $[(OiPr)_2Ti(BINOLate)_2]$ complex is disordered in three possible positions. Ti1 (1/4 occupancy) sits in general positions, and Ti2 (1/2 occupancy) sits on the two-fold axis along the *c* axis (Figure S13 in the Supporting Information). Every pair of L′ ligands shares a total of one $Ti(OiPr)_2$ fragment in Ti-**2**.

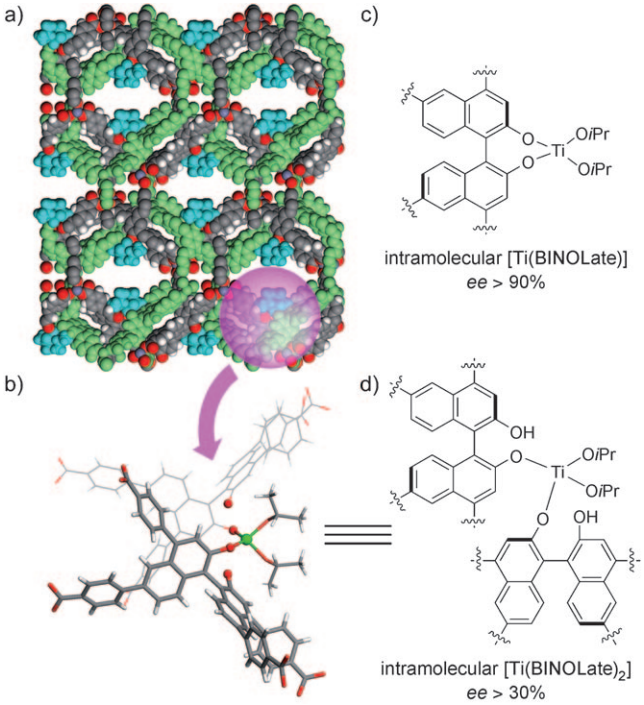

Figure 4. a) Space-filling model of framework Ti-**2**. $Ti(OiPr)_2$ blue, O red, C gray, H white; all atoms of the other interpenetrating network are shown in green. b) Stick and line model representation showing the X-ray structure of the intermolecular $[(OiPr)_2Ti(BINOLate)_2]$ species formed by crosslinking the two BINOL moieties in the two interpenetrating networks. Partially occupied $Ti(OiPr)_2$ fragments for the Ti1/T1A parts are omitted for clarity. Zn green, O red, C gray, H white. c) ChemDraw structure of the intramolecular $[(OiPr)_2Ti(BINOLate)]$ species. d) ChemDraw structure of the intermolecular $[(OiPr)_2Ti(BINOLate)_2]$ species.

Although Ti-**2** has the same space group as **2**, careful comparisons of their structures revealed significant changes in unit-cell dimensions and molecular conformations of the L′ ligands. The *a* and *b* axes of Ti-**2** increase by 3.1 % and 18.8 %, while the *c* axis shrinks by 12 % when compared to those of **2**. While the BINOL moieties in **2** adopt a transoid conformation with a dihedral angle of 111° between the naphthyl groups, the BINOL moieties adopt a cisoid conformation with a dihedral angle of 78.7° in Ti-**2**. In the structure of **2**, the hydroxy groups between adjacent BINOL moieties from two interpenetrating networks have the shortest hydroxy O–O distance of 3.74(2) Å. This O–O distance is shortened to 3.52(2) Å in Ti-**2**. In contrast, the two hydroxy groups in the same BINOL moiety in **2** have an O–O distance of 4.16(2) Å, which is too far away to simultaneously coordinate to a Ti center to form a $[(O\mathit{i}Pr)_2Ti(BINOLate)_2]$ complex. As a consequence of the crosslinking of the two interpenetrating networks by the Ti centers, the other inter-BINOL hydroxy O–O distance is shortened from 4.46(2) Å to 3.06(2) Å and also engages in forming intermolecular $[(O\mathit{i}Pr)_2Ti(BINOLate)_2]$ complexes (Figure S13 in the Supporting Information).

Space-filling models indicated the presence of substrate-accessible open channels in the framework Ti-**2** after the formation of intermolecular $[Ti(BINOLate)_2]$ species. We believe that the intermolecular $[Ti(BINOLate)_2]$ species should be less enantioselective in Et_2Zn addition reactions because of the smaller steric influence of the naphthyl rings on the Ti center. As a result, **2**/$Ti(O\mathit{i}Pr)_4$ exhibits much lower enantioselectivity than our previously reported MOF systems that can form desired intramolecular Ti BINOLate species (Figure 4c).[6,7,14] Control experiments with **1**/$Ti(O\mathit{i}Pr)_4$ indicated a significant background reaction that is non-enantioselective and further contributes to the low *ee* values observed for **2**/$Ti(O\mathit{i}Pr)_4$. To this end, when the loading of **2**/$Ti(O\mathit{i}Pr)_4$ was tripled, the *ee* value of the product increased from 17.4 % to 29.8 mol % (Table 1, entry 5). ICP-MS (ICP = inductively coupled plasma) analyses indicate the binding of Ti^{IV} to the framework of **2**, with a Ti/Zn ratio of 0.42.[15] The PXRD patterns of **2** remained essentially unchanged after Ti^{IV} loading and the Et_2Zn addition reaction, thus indicating that the framework crystallinity is well maintained during the catalytic reaction.

In conclusion, we have synthesized two 3D chiral MOFs based on tetracarboxylate bridging ligands and dizinc SBUs. Both MOFs **1** and **2** display very large 1D channels, even after twofold interpenetration, and exhibit high porosity, as characterized by N_2 and H_2 adsorption experiments. Modest enantioselectivity was observed for Et_2Zn addition reactions catalyzed by Ti-**2**. Single-crystal structure determination revealed that **2** underwent single-crystal to single-crystal crosslinking upon treatment with $Ti(O\mathit{i}Pr)_4$ to form intermolecular $[Ti(BINOLate)_2]$ complexes that are less enantiodiscriminating than intramolecular titanium BINOLate catalysts. This work highlights the important influence of framework structures on the enantioselectivity of MOF-derived asymmetric catalysts and the opportunity to obtain high-precision structural information of MOF-derived catalysts that is typically not available for their homogeneous counterparts. The rational design of MOF-derived catalysts can be greatly facilitated with the delineation of the relationship between their structures and catalytic properties.

Experimental Section

Synthesis of $[Zn_2L(DMF)(H_2O)]\cdot 4.3\,DMF\cdot 2\,EtOH\cdot H_2O$ (**1**): A mixture of ZnI_2 (31.9 mg, 0.10 mmol), H_4L (41.1 mg, 0.05 mmol), DMF (2 mL), and EtOH (2 mL) was heated in a capped vial at 90 °C for 3 days. Colorless crystals of **1** were filtered, and briefly dried on filter paper at room temperature. Yield: 46 mg (63 %). $[Zn_2L'(DMF)(H_2O)]\cdot 4.3\,DMF\cdot 2\,EtOH\cdot 4\,H_2O$ (**2**) was similarly synthesized in 51 % yield.

Diethylzinc addition experiments: Fresh prepared crystals of **2** (9.2 mg, 6.3 μmol) were washed repeatedly with anhydrous MeOH, CH_2Cl_2, and toluene. $Ti(O\mathit{i}Pr)_4$ (19 μL, 63 μmol) was added with vigorous stirring to the crystals of **2** suspended in toluene (1 mL). After 1 h, Et_2Zn (1.0 M in toluene, 147 μL, 147 μmol) and benzaldehyde (5 μL, 49 μmol) were added. The mixture was allowed to stir overnight, and then quenched by the addition of 1 mL of 3 M HCl. The organic layer was passed down a short silica column and analyzed by GC.

Received: June 3, 2010
Published online: September 21, 2010

Keywords: adsorption · asymmetric catalysis · crystal engineering · heterogeneous catalysis · metal–organic frameworks

[1] a) B. Moulton, M. J. Zaworotko, *Chem. Rev.* **2001**, *101*, 1629 – 1658; b) O. R. Evans, W. Lin, *Acc. Chem. Res.* **2002**, *35*, 511 – 522; c) S. L. James, *Chem. Soc. Rev.* **2003**, *32*, 276 – 288; d) N. W. Ockwig, O. Delgado-Friedrichs, M. O'Keeffe, O. M. Yaghi, *Acc. Chem. Res.* **2005**, *38*, 176 – 182; e) D. Bradshaw, J. E. Warren, M. J. Rosseinsky, *Science* **2007**, *315*, 977 – 980; f) G. Férey, *Dalton Trans.* **2009**, 4400 – 4415.

[2] a) M. Dincă, J. R. Long, *Angew. Chem.* **2008**, *120*, 6870 – 6884; *Angew. Chem. Int. Ed.* **2008**, *47*, 6766 – 6779; b) R. Matsuda, R. Kitaura, S. Kitagawa, Y. Kubota, R. V. Belosludov, T. C. Kobayashi, H. Sakamoto, T. Chiba, M. Takata, Y. Kawazoe, Y. Mita, *Nature* **2005**, *436*, 238 – 241.

[3] a) L. Ma, C. Abney, W. Lin, *Chem. Soc. Rev.* **2009**, *38*, 1248 – 1256; b) J. Lee, O. K. Farha, J. Roberts, K. A. Scheidt, S. T. Nguyen, J. T. Hupp, *Chem. Soc. Rev.* **2009**, *38*, 1450 – 1459.

[4] a) B. L. Chen, L. B. Wang, Y. Q. Xiao, F. R. Fronczek, M. Xue, Y. J. Cui, G. D. Qian, *Angew. Chem.* **2009**, *121*, 508 – 511; *Angew. Chem. Int. Ed.* **2009**, *48*, 500 – 503; b) A. J. Lan, K. H. Li, H. H. Wu, D. H. Olson, T. J. Emge, W. Ki, M. C. Hong, J. Li, *Angew. Chem.* **2009**, *121*, 2370 – 2374; *Angew. Chem. Int. Ed.* **2009**, *48*, 2334 – 2338; c) Z. Xie, L. Ma, K. E. deKrafft, A. Jin, W. Lin, *J. Am. Chem. Soc.* **2010**, *132*, 922 – 923.

[5] a) W. J. Rieter, K. M. Pott, K. M. L. Taylor, W. Lin, *J. Am. Chem. Soc.* **2008**, *130*, 11584; b) K. M. L. Taylor-Pashow, J. D. Rocca, Z. Xie, S. Tran, W. Lin, *J. Am. Chem. Soc.* **2009**, *131*, 14261; c) P. Horcajada, T. Chalati, C. Serre, B. Gillet, C. Sebrie, T. Baati, J. F. Eubank, D. Heurtaux, P. Clayette, C. Kreuz, J. S. Chang, Y. K. Hwang, V. Marsaud, P. N. Bories, L. Cynober, S. Gil, G. Ferey, P. Couvreur, R. Gref, *Nat. Mater.* **2010**, *9*, 172 – 178.

[6] a) C. Wu, A. Hu, L. Zhang, W. Lin, *J. Am. Chem. Soc.* **2005**, *127*, 8940 – 8941; b) C. Wu, W. Lin, *Angew. Chem.* **2007**, *119*, 1093 – 1096; *Angew. Chem. Int. Ed.* **2007**, *46*, 1075 – 1078.

[7] L. Ma, J. M. Falkowski, C. Abney, W. Lin, *Nat. Chem.* **2010**, DOI: 10:1038/nchem.738.

[8] The determination of the unit cell and data collections for colorless crystals of **1** and **2** were performed on a Siemens SMART CCD diffractometer. Data for Ti-**2** was collected on a Bruker SMART APEX II diffractometer. Crystallographic data for **1**: Orthorhombic, space group $I2_12_12_1$, $a=13.0884(3)$, $b=28.7131(7)$, $c=42.8771(11)$ Å, $V=16113.6(7)$ Å^3, $Z=8$, $\rho_{calcd}=0.858\ g\,cm^{-3}$, $\mu(Mo_{K\alpha})=0.635\ mm^{-1}$. $R1(I>2\sigma(I))=0.0713$, $wR2(I>2\sigma(I))=0.1513$, Flack parameter = 0.00(3) and GOF = 1.062. Crystallographic data for **2**: Orthorhombic, space group $I2_12_12_1$, $a=12.7526(10)$, $b=26.9066(19)$, $c=44.199(3)$ Å, $V=15166(2)$ Å^3, $Z=8$, $\rho_{calcd}=0.861\ g\,cm^{-3}$, $\mu(Mo_{K\alpha})=0.672\ mm^{-1}$. $R1(I>2\sigma(I))=0.0492$, $wR2(I>2\sigma(I))=0.1011$, Flack parameter = 0.10(1) and GOF = 0.890. Crystallographic data for Ti-**2**: Orthorhombic, space group $I2_12_12_1$, $a=13.1451(4)$, $b=31.9683(10)$, $c=39.8933(12)$ Å, $V=16344.0(9)$ Å^3, $Z=8$, $\rho_{calcd}=0.805\ g\,cm^{-3}$, $\mu(Cu_{K\alpha})=1.409\ mm^{-1}$. $R1(I>2\sigma(I))=0.0956$, $wR2(I>2\sigma(I))=0.2442$, Flack parameter = 0.10(6) and GOF = 1.223. CCDC 772189, 772190, and 778882 contain the supplementary crystallographic data for this paper. These data can be obtained free of charge from The Cambridge Crystallographic Data Centre via www.ccdc.cam.ac.uk/data_request/cif.

[9] a) V. A. Blatov, A. P. Shevchenko, V. N. Serezhkin, *Russ. J. Coord. Chem.* **1999**, *25*, 453 – 465; b) M. O'Keeffe, N. E. Brese, *Acta Cryst. A*, **1992**, *A48*, 663 – 669.

[10] C. Serre, F. Millange, C. Thouvenot, M. Noguès, G. Marsolier, D. Louër, G. Férey, *J. Am. Chem. Soc.* **2002**, *124*, 13519.

[11] a) K. K. Tanabe, S. M. Cohen, *Angew. Chem.* **2009**, *121*, 7560 – 7563; *Angew. Chem. Int. Ed.* **2009**, *48*, 7424 – 7427; b) M. Banerjee, S. Das, M. Yoon, H. J. Choi, M. H. Hyun, S. M. Park, G. Seo, K. Kim, *J. Am. Chem. Soc.* **2009**, *131*, 7524 – 7525.

[12] a) C. D. Wu, W. Lin, *Angew. Chem.* **2005**, *117*, 1994 – 1997; *Angew. Chem. Int. Ed.* **2005**, *44*, 1958 – 1961; b) L. R. MacGillivray, G. S. Papaefstathiou, T. Friscić, T. D. Hamilton, D. K. Bucar, Q. Chu, D. B. Varshney, I. G. Georgiev, *Acc. Chem. Res.* **2008**, *41*, 280 – 291; c) H. J. Park, M. P. Suh, *Chem. Eur. J.* **2008**, *14*, 8812 – 8821; d) B. D. Chandler, G. D. Enright, K. A. Udachin, S. Pawsey, J. A. Ripmeester, D. T. Cramb, G. K. Shimizu, *Nat. Mater.* **2008**, *7*, 229 – 235.

[13] Related catalytic reactions have recently been reported for molecular solids, see: a) A. N. Sokolov, D.-K. Bučar, J. Baltrusaitis, S. X. Gu, L. R. MacGillivray, *Angew. Chem.* **2010**, *122*, 4369 – 4373; *Angew. Chem. Int. Ed.* **2010**, *49*, 4273 – 4277; b) Z. Huang, P. S. White, M. Brookhart, *Nature* **2010**, *465*, 598 – 601.

[14] L. Pu, H.-B. Yu, *Chem. Rev.* **2001**, *101*, 757.

[15] The Ti content (Ti/Zn = 0.42) determined by the ICP-MS analysis is slightly higher than that determined from the X-ray structure (Ti/Zn = 0.25), thus suggesting that there might be some disordered, unreacted $Ti(OiPr)_4$ in the open channels of Ti-**2**.

